7. Cotton, F. A. & Walton, R. A. *Multiple Bonds between Metal Atoms* (Wiley & Sons, New York, 1982).
8. Roos, B. O. The ground state potential for the chromium dimer revisited. *Collect. Czech. Chem. Commun.* **68,** 265–274 (2003).
9. Roos, B. O. in *Advances in Chemical Physics; Ab Initio Methods in Quantum Chemistry – II* Ch. 69 (ed. Lawley, K. P.) 399–445 (Wiley & Sons, Chichester, 1987).
10. Andersson, K., Malmqvist, P.-Å., Roos, B. O., Sadlej, A. J. & Wolinski, K. J. Second-order perturbation theory with a CASSCF reference function. *Phys. Chem.* **94,** 5483–5488 (1990).
11. Pyykkö, P. Relativistic effects in structural chemistry. *Chem. Rev.* **88,** 563–594 (1988).
12. Karlström, G. *et al.* MOLCAS: a program package for computational chemistry. *Comput. Mater. Sci.* **28,** 222–239 (2003).
13. Gagliardi, L., Heaven, M. C., Wisborg Krogh, J. & Roos, B. O. The electronic spectrum of the UO_2 molecule. *J. Am. Chem. Soc.* (in the press).
14. Roos, B. O. & Malmqvist, P.-Å. Relativistic quantum chemistry–the multiconfigurational approach. *Phys. Chem. Chem. Phys.* **6,** 2919–2927 (2004).

Acknowledgements We thank P. Pyykkö and C. J. Cramer for comments on the manuscript, P.-Å. Malmqvist and B. E. Bursten for discussions, and V. Veryazov for graphical assistance. This work was partially supported by Ministero dell'Istruzione, dell'Università e della Ricerca (MIUR), the Swedish Research council (VR) and the Swedish Foundation for Strategic Research (SSF).

Competing interests statement The authors declare that they have no competing financial interests.

Correspondence and requests for materials should be addressed to L.G. (laura.gagliardi@unipa.it).

Lithospheric structure of the Rio Grande rift

David Wilson[1], Richard Aster[1], Michael West[2], James Ni[2], Steve Grand[3], Wei Gao[3], W. Scott Baldridge[4], Steve Semken[5] & Paresh Patel[3]

[1]*Department of Earth and Environmental Science and Geophysical Research Center, New Mexico Institute of Mining and Technology, Socorro, New Mexico 87801, USA*
[2]*Department of Physics, New Mexico State University, Las Cruces, New Mexico 88003, USA*
[3]*Jackson School of Geosciences, University of Texas, Austin, Texas 78712, USA*
[4]*Earth and Environmental Sciences Division, MS D462, Los Alamos National Laboratory, Los Alamos, New Mexico 87545, USA*
[5]*Department of Geological Sciences, Arizona State University, Tempe, Arizona 85287, USA*

A high-resolution, regional passive seismic experiment[1–6] in the Rio Grande rift region of the southwestern United States has produced new images of upper-mantle velocity structure and crust–mantle topography. Synthesizing these results with geochemical[7–9] and other geophysical[10–13] evidence reveals highly symmetric lower-crustal and upper-mantle lithosphere extensional deformation, suggesting a pure-shear rifting mechanism for the Rio Grande rift. Extension in the lower crust is distributed over a region four times the width of the rift's surface expression. Here we propose that the laterally distributed, pure shear extension is a combined effect of low strain rate and a regionally elevated geotherm, possibly abetted by pre-existing lithospheric structures, at the time of rift initiation. Distributed extension in the lower crust and mantle has induced less concentrated vertical mantle upwelling and less vigorous small-scale convection[14] than would have arisen from more localized deformation. This lack of highly focused mantle upwelling may explain a deficit of rift-related volcanics in the Rio Grande rift compared to other major rift systems such as the Kenya rift[15,16].

Rifting has a profound influence on continental evolution, fundamentally controlling crustal thinning and continental breakup. The character of a continental rift depends on how lithospheric strain is accommodated. Possible strain configurations range between pure-shear and simple-shear end members. The pure-shear model is characterized by ductile deformation of the lower crust and mantle lithosphere and predicts symmetric thinning and a symmetric lithospheric cross-section with respect to the rift axis[17]. The simple-shear model is characterized by strain localization along a master or a sequence of low-angle (10° to 30° dip) detachment(s) that may span the entire lithosphere[18]. A low-angle detachment predicts an asymmetric lithospheric cross-section, with the greatest crustal thinning laterally offset from greatest mantle lithosphere thinning.

In both the simple-shear and the pure-shear models, extensional thinning of crust and mantle lithosphere produces local upwelling of warm asthenosphere to replace thinned lithosphere. Additional heat is released by adiabatic decompression, producing partial melting and rift-associated volcanism. The emplacement of advected warmer material creates lateral temperature gradients that can induce small-scale convection[19,20]. Small-scale convective cells may create significant additional horizontal stresses that further advance rifting, volcanism and other lithosphere-scale deformation[14,20].

The simple-shear and pure-shear models offer distinct topographic, heat flow, gravity anomaly, and lithospheric velocity structural predictions. Ideally, it should be possible to distinguish between the models by the topographic expression of the rift, because the asymmetry of simple-shear deformation predicts asymmetry in the flexural uplift of the rift flanks[21], with the greatest uplift offset laterally from the surface expression of the rift. Rift-flank topography along the Rio Grande rift (RGR) (Fig. 1) is in fact relatively symmetric about the rift axis, with variations of typically less than 1–2 km between opposing rift flanks. However, the use of topography as a diagnostic tool may be significantly complicated by crustal composition and the fact that rifting has resulted in brittle deformation in the uppermost crust—expressed as a series of asymmetric grabens[15,22].

Similarly, the asymmetry of the simple-shear model predicts a complementary heat-flow asymmetry[23]. Heat-flow measurements in the RGR region show a broad region of roughly symmetric high heat flow trending approximately along the rift axis[24], consistent with pure-shear extension. However, regional heat-flow values along the RGR and elsewhere may be significantly complicated by advective hydrothermal transport within the crust.

One method of assessing the existence of simple-shear detachment(s) is to image the symmetry and location of maximum crustal thinning relative to the surface expression of the rift axis. We have constructed a new image of the crust–mantle boundary using receiver functions computed from teleseismic body waves recorded by the 950-km-long, 54-station LA RISTRA experiment[1–6], a linear transect that crossed the RGR obliquely near 34.5° (Fig. 1). Receiver function processing isolates P-to-S converted seismic phases generated by impedance discontinuities[25]. Discontinuity images are constructed by migration and stacking of many receiver functions with different ray paths through the crust and mantle, recorded at many stations. LA RISTRA receiver function images (Fig. 2) indicate crustal thickness ranging from 45 to 50 km beneath both the Colorado Plateau (stations NM34–UT54), and the Great Plains (TX01–NM20), with a rift-associated thinning to approximately 37 km centred beneath the RGR axis to within a few kilometres. These estimated crustal thicknesses are consistent with previous compilations of refraction surveys[26] across the RGR.

Using geologic constraints from previous seismic reflection work[24], we modelled the predicted geometry of the base of the crust (Moho) and the base of the lithosphere resulting from the amount of extension seen at the surface in the southern Albuquerque–Belen basin (16.9 km of extension over 60 km) (Figs 2, 3). The modelling technique[21] takes into account the kinematics of lithospheric extension, the isostatic response to crust and lithospheric thinning, and the elastic response of the lithosphere (flexure). Extension by either east- or west-dipping simple shear (Fig. 2a, b) predicts offset Moho upwarping that is

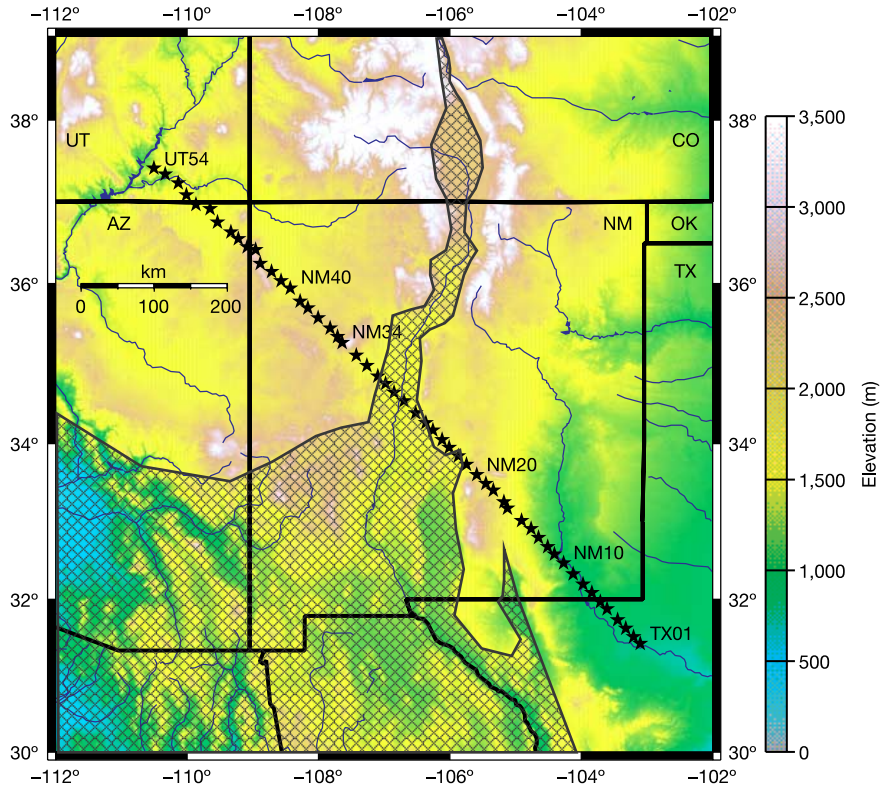

Figure 1 Elevation of the Rio Grande rift and surrounding region. The crosshatched pattern indicates the region of Cenozoic extension[15]. Stars indicate the broadband seismic stations of the LA RISTRA experiment. UT, Utah; AZ, Arizona; NM, New Mexico; CO, Colorado; OK, Oklahoma; TX, Texas.

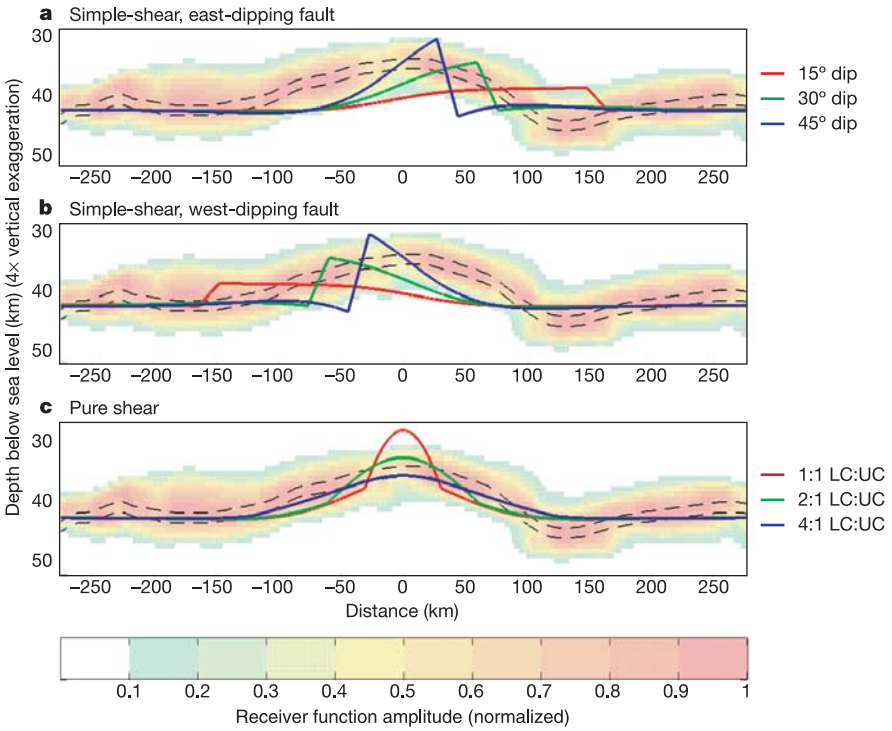

Figure 2 Modelled topography of the base of the crust. **a**, **b**, Predicted under simple shear extension for east-dipping faults (**a**) and west-dipping faults (**b**) with dips of 15°, 30° and 45°. **c**, Predicted from modelling pure-shear extension, with the lateral distribution of lower crustal extension relative to upper crustal extension (LC:UC) ranging from 1:1 to 4:1. For each LC:UC ratio, the volume of crustal thinning is the same. Underlying colours show positive migrated seismic receiver function amplitudes projected onto an east–west, rift-perpendicular profile. Dashed lines represent plus and minus one standard deviation crustal thickness (about 1.5 km).

significantly different from that observed, with the location of maximum crustal thinning offset laterally from the surface expression of the rift. The maximum misfit within 100 km of the rift axis between observed Moho depths and depths predicted by simple-shear extension for 15°, 30° and 45° east- and west-dipping faults is greater than 6 km for each case.

In contrast, modelling extension as pure shear (Fig. 2c) produces Moho upwarp that is centred on the rift axis and is highly consistent with the observed Moho geometry. Assuming that extension in the lower crust takes place over the same lateral distance (60 km) as in the upper crust (LC:UC = 1), sharp localized crustal thinning can occur, up to approximately 15 km, which is much greater and more localized than that observed. By allowing model extension in the lower crust to be distributed over a greater lateral distance we obtain more broadly distributed crustal thinning that is a much better fit to the observed Moho upwarp. A LC:UC ratio of 4:1 (lower crustal extension over 240 km laterally) gives the smallest maximum misfit of 1.8 km within 100 km of the rift.

An observation that complements the crustal thinning profile is the lithospheric thinning profile and its rift axis symmetry. Gravity data suggest thinning of the lithosphere near the rift axis[10], and previous regional teleseismic experiments[11–13] have noted increased teleseismic delay times, suggestive of an elevated lithosphere/asthenosphere boundary. In the central RGR, the elevated lithosphere/asthenosphere boundary is centred beneath the rift, but in the southern RGR the anomaly fans out to the southwest[13] as the RGR transitions into the Basin and Range province, a region of considerably greater Cenozoic extension. Geochemical analysis of volcanic rocks in the RGR region suggests asthenospheric ('depleted') magmatic source zones near the rift axis and lithospheric ('enriched')

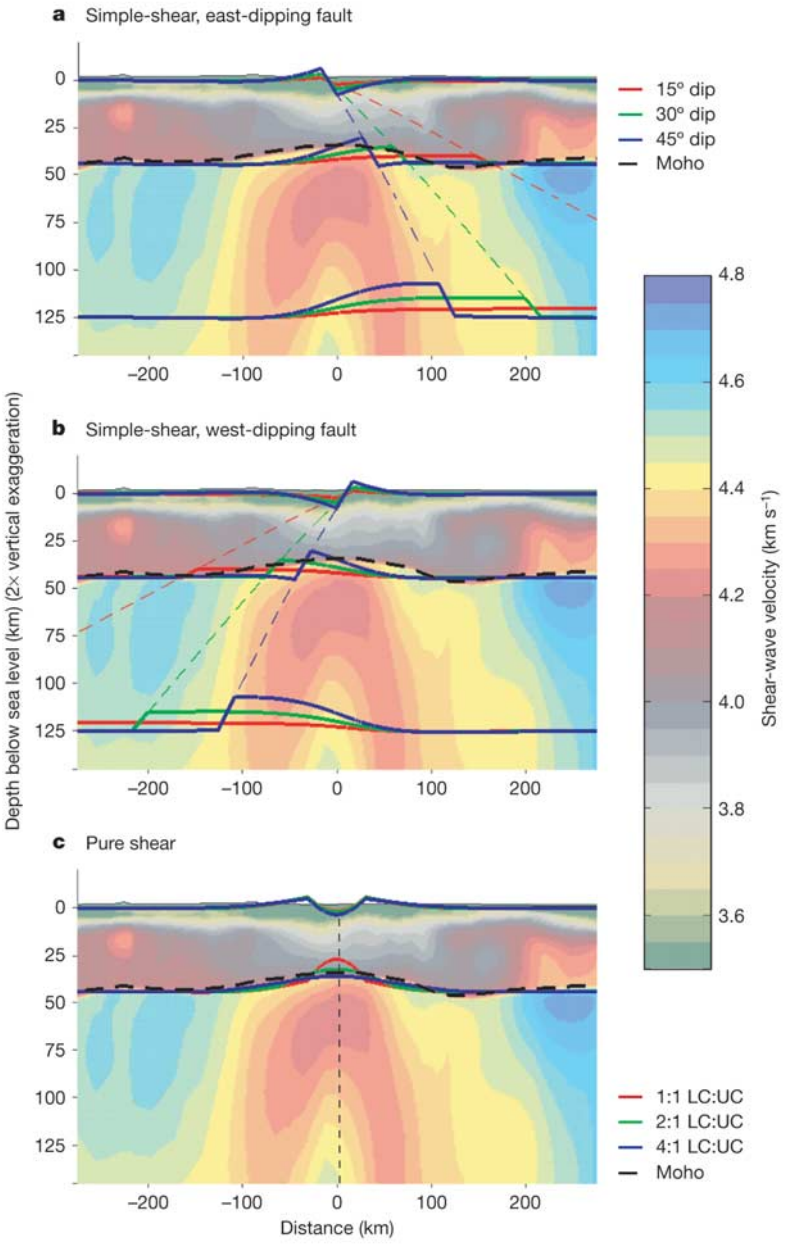

Figure 3 Lithospheric-scale cross-section in the identical projection used in Fig. 2, showing predicted surface topography and uplift of the Moho and lithosphere topography from modelling shown in Fig. 2. Underlying colours depict crust and upper-mantle shear-wave velocities determined from surface-wave phase velocity inversion[4]. Horizontal resolution of the surface wave velocity model is 55 km in the crust and 105 km in the upper mantle. The vertical dotted line in **c** denotes the rift axis. The centring of crust and mantle low velocities on the rift axis, and the symmetry of the low velocities, indicate symmetric mantle extension about the rift axis.

source zones on the outer flanks, further supporting thinned lithosphere roughly beneath the rift axis[7–9].

While each of the above lines of evidence suggests that lithospheric thinning is centred approximately beneath the rift axis, this study provides the first transect view of the crust, Moho and upper mantle. Inversion of LA RISTRA surface-wave dispersion indicates that shear velocities within 100 km of the rift axis are uniformly slow throughout the crust (Fig. 3). These velocities are probably the result of increased temperatures and the possible presence of melt[4]. The symmetry of the low velocities, and inferred thermal structure, are inconsistent with highly asymmetric crustal processes. Upper-mantle shear-wave velocities (Fig. 3) reveal a transition between high velocities beneath the Great Plains and Colorado plateau and a broad region of low velocities beneath the RGR. A similar pattern of low velocities centred beneath the rift is observed in P and S body tomography[2]. Modelled lithospheric upwarp due to simple shear extension (Fig. 3a, b) shows that the predicted location of maximum lithospheric upwarp for fault dips of 15°, 30° and 45° is offset from the rift axis by approximately 300, 180 and 100 km respectively for a reference lithospheric thickness of 125 km. Although the amount of lateral offset of maximum lithospheric upwarp depends on the reference lithospheric thickness used in modelling, simple-shear extension (Fig. 3a, b) predicts significant and observable offsets for a range of lithospheric thicknesses. Lithospheric thinning from pure shear extension, in contrast, predicts upwarp that is centred on the rift axis, and is aligned with the observed rift-centred low shear-wave velocity (Fig. 3c).

We performed numerical modelling[27] to compare predicted thermal and tectonic evolution of extending lithosphere by 28% over 200 km to our observed seismic imaging results. The crust is modelled as a plagioclase-rich material and the mantle is modelled as a dry olivine. Constraints on the magnitude and geometry of extension were taken from ref. 24. The modelling results show a relatively narrow zone of extension in the crust that is not matched by corresponding necking of the lithospheric mantle, where the deformation is nearly uniformly distributed. This result suggests that a pre-Cenozoic localized thermally elevated and/or compositionally weak zone was necessary to laterally concentrate strain in the mantle lithosphere underlying the RGR to the extent observed. The modelling results also show a thermal anomaly corresponding to a maximum shear-wave velocity anomaly of 2–3% (assuming $\partial \ln V_S/\partial T = -1.54 \times 10^{-4}\,\mathrm{K}^{-1}$)[28]. RISTRA velocity inversion, where regularization probably underestimates the true variability, indicates a relative mantle shear-wave velocity anomaly of at least 8% at depths of 50–100 km (Fig. 3). This discrepancy again highlights the need for pre-existing thermal and/or compositional mantle lithosphere anomalies to explain RGR evolution, localization and present structure.

The zone of low mantle velocities is considerably wider than the minimum horizontal resolution of 150 km (or 105 km, when projected to an east–west cross-section). Thus, mantle lithosphere deformation, although spatially concentrated relative to that modelled from uniform starting conditions, is resolved to be distributed over a substantially greater lateral distance than at the surface (Fig. 3c). Major factors controlling whether lithosphere will deform by localized brittle deformation, or by distributed ductile deformation are rheology, temperature and strain rate[29]. High temperatures and low strain rates are conducive to ductile deformation. A regionally elevated geotherm during rift initiation[29] is suggested by widespread regional ignimbrite volcanism around 30 Myr ago. This event, probably caused by the foundering of the subducting Farallon slab and corresponding return asthenospheric flow[30], may have created a zone of thermally weakened lithosphere beneath the region. Cenozoic strain rates in the central RGR are also relatively low, with only 18–28% total extension (16.9 km extension over 60 km in the southern Albuquerque–Belen basin) during the last 30 Myr[22,24], although strain accumulation may have been concentrated in two distinct periods, 30–18 Myr ago and 10–5 Myr ago[22]. Even so, this suggests RGR formational strain rates of only 10^{-16} to $10^{-15}\,\mathrm{s}^{-1}$ (0.56 to 1 mm yr^{-1}). This low strain rate, along with increased temperature, may have enabled ductile deformation of the lithosphere, producing the observed symmetric region of laterally distributed pure-shear deformation. Although volumes of lithospheric thinning and upwelling mantle are the same for distributed versus concentrated deformation scenarios, the observed lateral distribution of lithospheric deformation over a region that is approximately four times the width of the rift's surface expression may have resulted in less concentrated vertical mantle upwelling. The lateral temperature gradients that would have been produced by distributed extension are smaller than those expected for concentrated extension, inducing less vigorous small-scale convection and thus limiting the amount of heat delivered advectively to the shallow rift. As a result, the RGR has experienced relatively small volumes of rift-related volcanism when compared to other rift systems (for example, RGR extrusives are only 5–10% of the Kenya rift)[15,16]. □

Received 26 February; accepted 6 December 2004; doi:10.1038/nature03297.

1. Wilson, D. *et al.* Broadband seismic background noise at temporary seismic stations observed on a regional scale in the southwestern United States. *Bull. Seismol. Soc. Am.* **92,** 3335–3341 (2002).
2. Gao, W. *et al.* Upper mantle convection beneath the central Rio Grande rift imaged by P and S wave tomography. *J. Geophys. Res.* **109,** doi:101029/2003JB002743 (2004).
3. Gök, R. *et al.* Shear wave splitting and mantle flow beneath LA RISTRA. *Geophys. Res. Lett.* **30,** doi:101029/2002GL016616 (2003).
4. West, M. *et al.* Crust and upper mantle shear wave structure of the southwest of the southwest United States: Implications for rifting and support for high elevation. *J. Geophys. Res.* **109,** doi:101029/2003JB002575 (2004).
5. Wilson, D. *et al.* Imaging crust and upper mantle seismic structure in the southwestern United States using teleseismic receiver functions. *Leading Edge* **22,** 232–237 (2003).
6. Wilson, D. *et al.* Seismic structure of the lithosphere in the southwestern United States using teleseismic receiver functions. *J. Geophys. Res.* (submitted).
7. Perry, F. V., Baldridge, W. S. & DePaolo, D. J. Chemical and isotopic evidence for lithospheric thinning beneath the Rio Grande rift. *Nature* **332,** 432–434 (1998).
8. Baldridge, W. S. *et al.* Middle to Late Cenozoic magmatism of the southeastern Colorado plateau and central Rio Grande rift (New Mexico and Arizona, USA)—A model for continental rifting. *Tectonophysics* **197,** 327–354 (1991).
9. McMillan, N. J. Temporal and spatial magmatic evolution of the Rio Grande rift. *New Mexico Geol. Soc. Guidebk* **49,** 107–116 (1998).
10. Cordell, L., Zorin, Y. A. & Keller, G. R. The decompensative gravity anomaly and deep structure of the region of the Rio Grande rift. *J. Geophys. Res.* **96,** 6557–6568 (1991).
11. Parker, E. C., Davis, P. M., Evans, J. R., Iyer, H. M. & Olsen, K. H. Upwarp of anomalous asthenosphere beneath the Rio Grande rift. *Nature* **312,** 354–356 (1984).
12. Davis, P. M. Continental rift structures and dynamics with reference to teleseismic studies of the Rio Grande and East-African rifts. *Tectonophysics* **197,** 309–325 (1991).
13. Slack, P. D. *et al.* The upper mantle structure of the central Rio Grande Rift region from teleseismic P- and S- wave travel time delays and attenuation. *J. Geophys. Res.* **101,** 16003–16023 (1996).
14. Mutter, J., Buck, W. R. & Zehnder, C. Convective partial melting. 1. A model for the formation of thick basaltic sequences during the initiation of spreading. *J. Geophys. Res.* **93,** 1031–1048 (1988).
15. Olsen, K. H., Baldridge, W. S. & Callender, J. F. Rio Grande rift: an overview. *Tectonophysics* **143,** 119–139 (1987).
16. Keller, G. R. *et al.* A comparative study of the Rio Grande and Kenya rifts. *Tectonophysics* **197,** 355–371 (1991).
17. McKenzie, D. Some remarks on the development of sedimentary basins. *Earth Planet. Sci. Lett.* **40,** 25–32 (1978).
18. Wernicke, B. Uniform sense normal simple shear of the continental lithosphere. *Can. J. Earth Sci.* **22,** 108–125 (1985).
19. Buck, R. W. Small-scale convection induced by passive rifting: the cause for uplift of rift shoulders. *Earth Planet. Sci. Lett.* **77,** 362–372 (1986).
20. Huismans, R. S., Podladchikov, Y. Y. & Cloetingh, S. Transition from passive to active rifting: Relative importance of asthenospheric doming and passive extension of the lithosphere. *J. Geophys. Res.* **106,** 11271–11291 (2001).
21. Weissel, J. K. & Karner, G. D. Flexural uplift of rift flanks due to mechanical unloading of the lithosphere during extension. *J. Geophys. Res.* **94,** 13919–13950 (1989).
22. Chapin, C. E. & Cather, S. M. Tectonic setting of the axial basins of the northern and central Rio Grande rift. *Geol. Soc. Am. Spec. Pap.* **291,** 5–24 (1994).
23. Buck, R. W., Martinez, F., Steckler, M. S. & Cochran, J. R. Thermal consequences of lithospheric extension: pure and simple. *Tectonics* **7,** 213–234 (1988).
24. Russell, L. R. & Snelson, S. in *Interior Rift Basins* (ed. Landon, S.) *AAPG Mem.* **59,** 205–258 (1994).
25. Langston, C. A. Corvallis, Oregon, crustal and upper mantle receiver structure from teleseismic P and S waves. *Bull. Seismol. Soc. Am.* **67,** 713–724 (1977).
26. Keller, G. R. & Baldridge, W. S. The Rio Grande rift: A geological and geophysical review. *Rocky Mountain Geol.* **34,** 131–148 (1999).
27. Lavier, L. L. & Buck, W. R. Half graben versus large-offset low-angle normal fault: importance of keeping cool during normal faulting. *J. Geophys. Res.* **107,** ETG 8-1–13 (2002).
28. Karato, S. Importance of anelasticity in the interpretation of seismic tomography. *Geophys. Res. Lett.* **20,** 1623–1626 (1993).

29. Morgan, P., Seager, W. & Golombek, M. Cenozoic thermal, mechanical and tectonic evolution of the Rio Grande rift. *J. Geophys. Res.* **91,** 6263–6276 (1986).
30. Humphreys, D. Post-Laramide removal of the Farallon slab, western United States. *Geology* **23,** 987–990 (1995).

Acknowledgements We thank G. R. Keller and Roger Buck for comments. Field and data handling assistance was provided by the IRIS PASSCAL Instrument Center at the New Mexico Institute of Mining and Technology (NMT). This research was supported by NSF grants, the Los Alamos National Laboratory Institute for Geophysics and Planetary Physics, the New Mexico State University Arts and Sciences Research Center, and the NMT Geophysical Research Center. A permit is necessary to conduct geological investigations on the Navajo Nation from the Navajo Nation Minerals Department.

Competing interests statement The authors declare that they have no competing financial interests.

Correspondence and requests for materials should be addressed to D.W. (davew@ees.nmt.edu).

Counter-rotating microplates at the Galapagos triple junction

Emily M. Klein[1], Deborah K. Smith[2], Clare M. Williams[2] & Hans Schouten[2]

[1]*Nicholas School of the Environment and Earth Sciences, Duke University, Durham, North Carolina 27708-0227, USA*
[2]*Woods Hole Oceanographic Institution, Woods Hole, Massachusetts 02543, USA*

An 'incipient' spreading centre east of (and orthogonal to) the East Pacific Rise at 2° 40′ N has been identified as forming a portion of the northern boundary of the Galapagos microplate[1,2]. This spreading centre was described as a slowly diverging, westward propagating rift, tapering towards the East Pacific Rise. Here we present evidence that the 'incipient rift' has also rifted towards the east and opens anticlockwise about a pivot at its eastern end. The 'incipient rift' then bounds a second microplate, north of the clockwise-rotating Galapagos microplate. The Galapagos triple junction region, in the eastern equatorial Pacific Ocean, thus consists of two counter-rotating microplates partly separated by the Hess Deep rift. Our kinematic solution for microplate motion relative to the major plates indicates that the two counter-rotating microplates may be treated as rigid blocks driven by drag on the microplates' edges[3].

The development of the Galapagos microplate (GMP) in the eastern equatorial Pacific Ocean begins with the confluence of the Cocos–Nazca, Pacific–Nazca and Pacific–Cocos spreading centres, forming a diffuse triple junction (Fig. 1b inset). Lonsdale[1] proposed that isolation of ocean crust generated at the East Pacific Rise (EPR) initiated in the south at ~1 Myr ago with the growth of a prominent seamount adjacent to the Pacific–Nazca spreading centre. This led to a zone of weakness and magma upwelling between the seamount and the adjacent EPR, forming a short, east–west-trending spreading centre. Over time, this spreading centre propagated northeastwards, becoming the Nazca–Galapagos spreading centre. In the current plate configuration, this plate boundary widens and deepens as it approaches the southern bounding scarps of the Galapagos gore, near 101° W, in what is called the Dietz Deep.

In contrast to the relatively well-understood southern boundaries of the GMP, the configuration of its northern boundary has not been fully elucidated. Early studies suggesting that the northern boundary consisted of the westward extension of the Cocos–Nazca spreading centre[4,5] were later refuted by the finding that the Cocos–Nazca spreading centre does not link to the EPR, but rather terminates ~50 km east of it at the Hess Deep[6,7]. Subsequent surveys further north, however, identified the 'incipient rift' (IR), a magmatically active, newly forming, spreading centre east of and orthogonal to the EPR at ~2° 40′ N (refs 1, 2, 8), forming at least a portion of the northern boundary of the GMP. A study of the western portion of the IR suggested that it consists of a slowly diverging (~15 mm yr^{-1}), westward propagating, spreading centre between the Cocos and Galapagos plates, which leaves a wedge-shaped gore in its wake[2].

In August 2002, aboard the R/V *Melville*, we mapped and sampled a broad region centred on the IR, including its intersection with the EPR and extending ~140 km to the east. Various geological, geophysical and rock sampling tools were used, including SeaBeam2000 bathymetry and side-scan (amplitude) coverage; towed magnetometer; bottom photography (14 camera tows using the WHOI Towed Camera System); water column hydrothermal surveying[9]; and rock sampling[10]. Here we present findings based primarily on our bathymetric, side-scan, magnetic and camera tow results.

The east–west-trending IR is shallowest (~2,900 m below sea level) near its intersection with the EPR (at ~2° 40′ N), and deepens progressively eastward (>3,500 m), exceeding average depths of ambient sea floor to its north (Fig. 1a). The loci of greatest depths along the eastern half of the IR form a sinuous trough that trends ~100° to the southeast. SeaBeam amplitudes for the IR indicate high reflectivity consistent with relatively sparse sediment cover compared to adjacent sea floor (Fig. 2a). Along the eastern portion of the IR, reflection amplitudes delineate an eastward-narrowing, highly reflective 'wedge' that coincides with the location of the bathymetric trough. The apex of this wedge clearly cuts north–south-oriented abyssal hills and then dies out in the vicinity of 101° 30′ W (Fig. 2a).

The photographic and magnetic data support the idea that the IR, including the eastern reflective trough, is magmatically active. Photographs of the crust along the IR show sparsely sedimented lavas, often with delicate ornamentation and basaltic glass (recovered by dredging), with local in-filling of sediment between pillows (Fig. 2a–c). In a number of photographs, particularly along the eastern portion of the IR, lavas appear to emanate from local fissures with east–west orientations (for example, Fig. 2b). Previous studies of northern EPR crust show that within a few kilometres of the ridge axis, undisturbed lavas generally become buried under a thick pile of sediment[11]. Although not as fresh as lavas observed at recent EPR axial eruptions, the lavas photographed along the eastern IR appear significantly younger than the calculated crustal age of ~400–700 kyr (based on the EPR spreading rate), and therefore probably erupted *in situ*. In the absence of radiometric age dates, we speculate that these lavas are a few thousand years old, based on age-dating studies performed on lavas photographed in place elsewhere[11]. This suggests that although the IR is magmatically active along its length, it may be only sporadically so, interspersed with periods of magmatic inactivity and sediment burial, consistent with its slow spreading rate.

Magnetic anomaly profiles run over the IR also support recent magmatic activity (Fig. 1b). Using magnetic field data (collected on our own cruise and on previous cruises), we calculated crustal magnetization, taking into account bathymetry and assuming a constant source thickness of 0.5 km (refs 12, 13). A crustal magnetization high is centred over the IR at ~101° 43′ N, which can be explained by a thicker magnetic source layer, younger and therefore more highly magnetized rocks (for example, erupted <10 kyr ago), and/or lavas with higher Fe or Ti contents than the surrounding region. The higher iron contents of basalts (13–16 wt% Fe_2O_3)[10] dredged from this region can explain only half the amplitude of the magnetization[14]. We suggest that the other half is caused by the high magnetization of young lavas that record the high geomagnetic field intensity of the past 10 kyr (ref. 15).

The fact that the eastern portion of the reflective IR wedge cuts north–south-oriented abyssal hills, combined with the side-scan, magnetic and camera-tow data suggesting recent magmatism along